Available online at www.sciencedirect.com
ScienceDirect
Journal of Sound and Vibration 297 (2006) 492–511
JOURNAL OF SOUND AND VIBRATION
www.elsevier.com/locate/jsvi

Noise reduction in a flow duct: Implementation of a hybrid passive/active solution

N. Sellen[1], M. Cuesta[2], M.-A. Galland*

Laboratoire de Mécanique des Fluides et d'Acoustique UMR CNRS 5509, Ecole Centrale de Lyon, 69134 Ecully Cedex, France

Received 16 May 2005; received in revised form 20 March 2006; accepted 30 March 2006
Available online 21 June 2006

Abstract

This paper deals with the design of a hybrid acoustic treatment combining porous material properties and active control techniques. Such an acoustic system was studied with a view to reducing broadband noise spectra in flow duct applications. Special attention was paid to the selection of the passive layer. The main objective was to achieve target impedance at the front absorber face, so as to attain maximum sound-attenuation over a wide frequency bandwidth. This investigation was carried out for a specific laboratory flow duct. Different porous layers were studied to reproduce optimum impedance at the hybrid liner surface. Results showed the difficulty of simultaneously achieving optimum resistance and reactance. Thus, a compromise was struck by applying a criterion of maximum attenuation. A wire mesh with a resistance close to a third of the characteristic impedance of air was selected as the optimal passive layer. Experiments were carried out in the flow duct under grazing acoustic incidence and with flow velocities up to 50 m/s. The experimental transmission loss was in agreement with predictions. Significant noise reduction levels were achieved throughout a large frequency range from 0.7 to 2.5 kHz, with a cut-off frequency between active and passive mode set at 1.8 kHz.

1. Introduction

The recent development of automotive and aircraft transport has contributed to the emergence of a new kind of nuisance: noise pollution. In aeronautics in particular, ever more severe regulations have been drawn up by the International Civil Aviation Organization (ICAO). Acoustic certification procedures have thus been introduced, imposing noise restrictions, leading to the setting up of many European and American aircraft noise reduction research programs. An important contribution comes from turbo engines—and more precisely from the fan, in the specific case of modern high bypass-ratio engines. This noise spectrum is characterised by pure tones (BPF and its harmonics) over a broadband component, both depending on the operating regime of the turbo engine. Noise can be reduced by certain absorbent treatments applied to the nacelle walls.

*Corresponding author. Tel.: +33 0 4 72 18 60 13; fax: +33 0 4 72 18 91 43.
E-mail address: Marie-Annick.Galland@ec-lyon.fr (M.-A. Galland).
[1]Presently at SNECMA Moteurs, Site de Villaroche, Departement Acoustique, 77550 Moissy-Cramayel, France.
[2]Presently at Instituto de Acustica, Consejo Superior de Investigaciones Cientificas (CSIC), Madrid, Spain.

0022-460X/$ - see front matter © 2006 Elsevier Ltd. All rights reserved.
doi:10.1016/j.jsv.2006.03.049

The present study concerned the design of a new kind of liner, to limit fan noise propagating in the turbo engine inlet. This acoustic treatment consists of a hybrid absorbent cell, combining passive properties of a porous material and active control to ensure pressure cancellation at the rear face of the porous sheet. The hybrid absorption concept refers to the double operation of the cell: active at low and passive at higher frequencies. Such an acoustic system is intended to enlarge the frequency bandwidth treated, compared to existing acoustic liners. Conventional passive treatments (single degree of freedom: sdof; 2 degrees of freedom: 2dof) afford high attenuation levels over a rather narrow frequency range, while purely active technologies appear to be effective mainly at low frequencies.

The notion of active absorption was firstly introduced by Olson and May [1] who proposed an *electronic sound absorber* providing pressure release on the back face of a resistive sheet. In the 1980s, Guicking and Lorenz [2] validated this concept experimentally. Many investigations have sought to implement hybrid absorption technology, leading to patent applications [3]. Thenail [4] and Furstoss [5] developed an active treatment composed of a glass wool layer backed by an air cavity closed through an active surface. Beyene and Burdisso [6] achieved active boundary conditions by means of impedance adaptation in a porous rear face layer. Recently, Cobo et al. [7] demonstrated the feasibility of designing thinner hybrid passive/active absorbers using microperforated panels rather than the conventional porous materials.

For aeronautic applications, many constraints related to the hostile nacelle environment have to be taken into account to manufacture a reliable and resistant hybrid liner. Among the mechanical, climatic and geometrical constraints, treatment performance has to integrate weight, shape and reliability factors as well as easy replacement of the absorbent cells in case of damage. Initial broadband noise spectrum reduction studies were run by the *Centre Acoustique du LMFA, Ecole Centrale de Lyon* in the framework of the European RANNTAC (Reduction of Aircraft Noise by Nacelle Treatment and Active Control) and RESOUND (Reduction of Engine Source Noise through Understanding and Novel Design) projects. An active absorbent cell composed of a resistive layer backed by an active control module was developed and validated under normal acoustic incidence. Further experiments by Galland [8] and [9] on a flow duct under grazing acoustic incidence led to pressure reductions up to 10 dB outside the test bench. Several resistive layers were moreover applied to the cell's front face, enabling power reduction up to 12 dB in the no-flow configuration.

The present study concerns the European SILENCER (Significantly lower community exposure to aircraft noise GRD1-2000-25297) programme, which seeks to design new technologies ensuring attenuation of perceived aircraft noise. As acoustic treatments are generally characterised by their surface impedance, the hybrid active/passive liner has been specifically developed to reach a pre-targeted impedance on the front absorber face. The goal of the present investigation was to optimise the hybrid acoustic treatment in the more general case of flow duct applications. A specific experimental set-up was designed to further estimate and validate the proposed strategy. Both the active and passive components of the hybrid liner were optimised to achieve maximum noise reduction in the laboratory. The present paper focuses on the passive layer optimisation. The complementary active control system has been analysed in Refs. [10,11]. Promising attenuation results were obtained with the hybrid absorbent cells [12].

Both the general description of a hybrid passive/active absorber and the procedure to optimise the proposed hybrid cell are available in Section 2. The characteristics of the optimum impedance of such a liner and the theoretical approach to implement it are presented in Sections 3 and 4, respectively. Finally, the effectiveness of the hybrid technology under grazing acoustic incidence is experimentally demonstrated in Section 5.

2. Hybrid cell optimisation procedure

The basic principle of the active absorber was previously described and validated in Ref. [5]. It results from the low-frequency behaviour of a porous material, which mainly depends on its flow resistance R or its resistivity σ as follows:

$$R = \frac{P_1 - P_2}{V} = \sigma e, \tag{1}$$

where e is the thickness of the porous sample, and V the velocity of the air flow through the material due to the pressure gradient $\Delta P = P_1 - P_2$. When the acoustic pressure P_2 at the rear porous sheet face is cancelled, the

material surface impedance $Z = P_1/V$ becomes proportional to resistivity (2)

$$Z = \frac{P_1}{V} = \sigma e. \tag{2}$$

Under such conditions, i.e. $P_2 = 0$, the surface impedance, or more precisely the surface resistance, of a given porous medium can easily be controlled with a suitable thickness e. For instance, the maximal absorption in case of normal incidence is reached for a purely real impedance equal to the characteristic impedance of air Z_0. The acoustic pressure on the rear porous sheet face can be cancelled, placing the material at a quarter of a wavelength from a rigid wall. This technique is commonly used to design conventional passive treatments. Such methods nevertheless present many drawbacks, since the frequency range in which the pressure release is achieved remains quite narrow. Moreover, at low frequencies, the air gap behind the porous material becomes rather significant (for instance: at 500 Hz, $\lambda/4 = 0.17$ m). However, the pressure release condition behind the material can be also provided by an active control system composed of a secondary source, a controller and a control microphone, as suggested by Olson [1].

A hybrid active/passive liner can therefore be achieved by connecting hybrid cells (see Fig. 1), each comprising a porous layer backed by an active control system. The main advantage of such a hybrid treatment is to absorb over a wider frequency bandwidth without increasing system bulk. The hybrid operation can be summarised as follows: at low frequencies, the active control on the rear material face is turned on (*active functioning mode*), ensuring the pressure release condition (see Fig. 2(a)). Thus, the surface impedance of the porous layer becomes purely resistive, and is governed by the resistivity of the medium. In the higher frequency range, the active control system is turned off (*passive functioning mode*) and the porous layer is therefore backed by an air cavity of optimised depth (see Fig. 2(b)).

This treatment appears to be well suited to flow duct applications, even in the active functioning mode, since the active part is protected from the flow by the porous layer. The objective of this study was to define, build and test an active/passive liner optimised for a dedicated laboratory flow duct. The MATISSE test bench (Fig. 3) consisted of a 3.20 m long square cross-section duct ($66 \times 66\,\text{mm}^2$) with anechoic termination. Such small transverse dimensions led to a large plane wave analysis up to approximately 2.5 kHz in the flow duct. A silent flow generator at the upstream extremity induced mean flow velocities up to 50 m/s. The acoustic source was mounted on the upper wall, upstream of the acoustic treatment. The liner of finite length was assumed to be locally reacting, and could be applied either on the upper wall or on both opposite walls of the duct.

The optimal hybrid absorbent cell for MATISSE was implemented following the global optimisation procedure described in Fig. 4. First, the optimum impedance to be reached at the input of the hybrid liner was characterised. Then, a theoretical study concerning the parallel optimisation of both passive and active

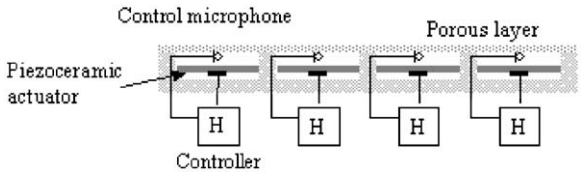

Fig. 1. The hybrid active/passive treatment.

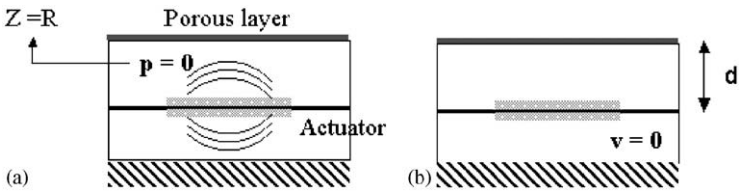

Fig. 2. Hybrid active/passive functioning modes of the acoustic absorbent cell: (a) at low frequencies: active mode and (b) at high frequencies: passive mode.

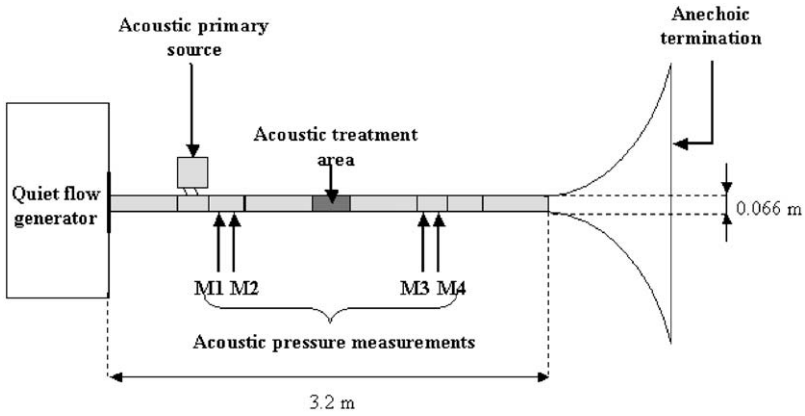

Fig. 3. MATISSE flow duct.

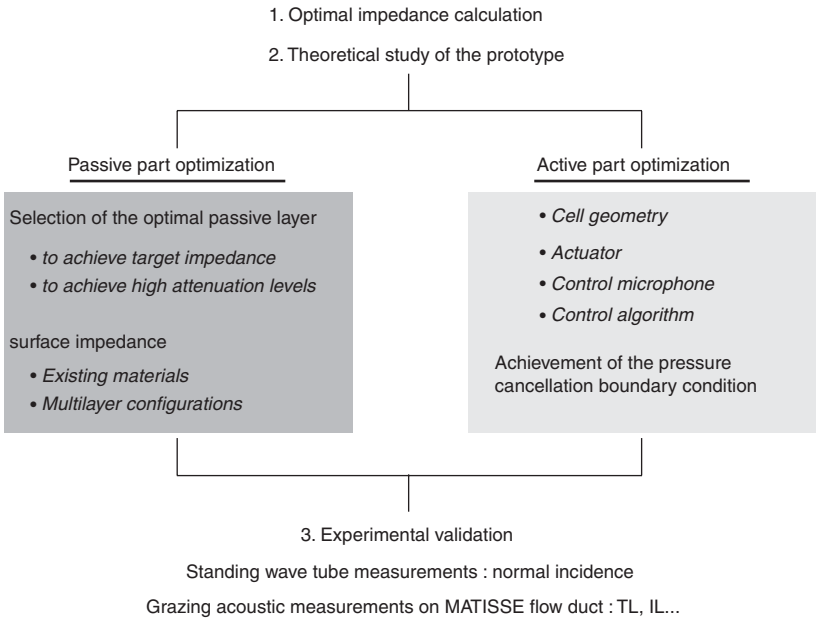

Fig. 4. Hybrid cell optimisation procedure.

components was conducted. Note that only the passive optimisation step has been included in the present paper. Therefore, a reliable pressure release condition behind the porous sheet was assumed for the active control functioning. The passive optimisation stage involved the selection of the best-suited porous layer so as to reproduce the optimum impedance as well as to provide maximum sound attenuation levels. Finally, this hybrid technology was validated, under normal acoustic incidence in a standing wave tube and under grazing acoustic incidence on the MATISSE flow duct.

3. Optimum impedance

Any acoustic treatment is generally characterised by its surface impedance. For the specific MATISSE flow duct configuration, the first goal was to define the optimum impedance of the liner, leading to maximum

attenuation downstream of the treatment. Accordingly, a complete description of the sound propagation inside a constant cross-sectional flow duct was necessary.

The sound pressure field at any position of an infinite or semi-infinite duct with at least one treated wall has been calculated by many authors [13,14]. The notion of optimum impedance was introduced by Cremer [15]. This approach was restricted to rectangular ducts with the entire upper wall covered by the acoustic treatment. Cremer revealed the frequency evolution of the optimum impedance for the considered test bench. The optimum resistance and reactance of the liner were of the same order under a grazing acoustic incidence. Conversely the maximum attenuation in case of a plane wave impinging under normal incidence was reached with a purely resistive impedance. Later, Tester generalised Cremer's results to flow ducts [16]. The main difficulty concerned the correct implementation of the boundary condition on the absorbent wall, [17,18]. The mass, velocity, and energy conservative equations were solved by simulation. Recent studies based on finite element methods considered more realistic flow profiles [19] and showed that numerous factors, such as source specifications, may influence optimum impedance.

In the present study, the optimum impedance of the lining treatment was calculated for the MATISSE facility (Fig. 3). This parameter was evaluated with a performance index estimating the noise reduction levels downstream of the absorber. Both the insertion loss and transmission loss factors are commonly considered in flow duct applications [14,20]. The transmission loss was particularly well suited to the MATISSE facility due to the anechoic termination and to the plane wave domain here considered.

The acoustic pressure field inside MATISSE was estimated by a multimodal expansion model, previously described by Thenail [4] in the no-flow condition. To characterise such absorbers under flow, a simplified sound propagation model introducing a uniform mean flow was then tested. For the set-up under consideration, this modal expansion tool was sufficient to predict the liner behaviour on the duct wall, and to further compare both theoretical and experimental performance. A different problem—involving complex geometries or higher flow velocities, for instance—would require a more realistic description to achieve accurate prediction. In those conditions, more robust sound propagation models [18,21] and a reliable implementation of the finite impedance boundary condition [17] would have to be adopted, since boundary layer effects cannot be neglected in most industrial applications [22].

3.1. Theoretical hypothesis and basis

Both acoustic pressure and velocity fields were determined in a 3D (x, y, z) duct characterised by two transverse dimensions, $L_x = L_y = 0.066\,\text{m}$, and one longitudinal value, $L_z = 3.20\,\text{m}$. Fig. 5 illustrates the calculation set-up in the uniform mean flow case. The simulated duct was divided into three zones with diverse boundary conditions along their walls.

The first, Zone I, corresponded to the primary acoustic source region. The duct walls were entirely rigid. The second, Zone II, was the treated region, of variable length. The liner, characterised by its finite impedance Z, could be applied to either the upper wall ($y = L_y/2$) or both opposite duct walls ($y = -L_y/2$ and $y = L_y/2$). The third, Zone III, corresponded to the anechoic termination downstream of the acoustic treatment. The duct walls were rigid.

The acoustic source was modelled as a velocity piston located at the inlet transverse plane ($z = 0$). Although in the experimental set-up the primary source was situated on the upper wall, the simulation remained close to the measurement configuration, as it was assumed that the plane wave was fully established at this location. The no flow case was completely solved for plane waves (frequency below 2.5 kHz) and high-order modes and the acoustic field convergence verified. For instance, a parametric study showed that 10 modes were sufficient

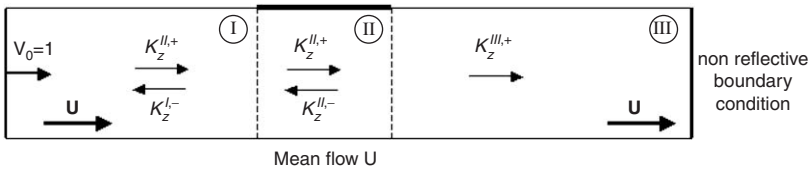

Fig. 5. Calculation configuration.

to accurately approximate the acoustic propagation inside the duct up to 5 kHz. Concerning the uniform mean-flow configuration, simulations were carried out assuming only the plane mode propagating inside MATISSE duct. The time dependance $e^{i\omega t}$ is assumed.

In each of these zones, the acoustic potential $\Phi^i(x,y,z)$ ($i = \mathrm{I}, \mathrm{II}, \mathrm{III}$) can be expressed as follows:

$$\Phi^i(x,y,z) = \sum_m \sum_n \Phi^i_{mn}(x,y)[A^i_{mn} e^{-jk^{i,+}_{z,mn}z} + B^i_{mn} e^{jk^{i,-}_{z,mn}z}]. \tag{3}$$

The indices m and n are the mth x-transverse mode, which is analytically expressed, and nth y-transverse mode, which has to be numerically determined in the general case. The y-dependent contributions of the eigenfunctions Φ^i_{mn} are deduced from the transverse Helmholtz equation (4), taking into account the associated boundary condition on the duct walls.

$$\begin{cases} \dfrac{d^2\psi^{\mathrm{II}}}{dy^2} + (k_y^{\mathrm{II}})^2\psi^{\mathrm{II}} = 0, \\ \dfrac{d\psi^{\mathrm{II}}}{dy}\Big|_{y=-\frac{L_y}{2}} = 0, \\ \dfrac{d\psi^{\mathrm{II}}}{dy}\Big|_{y=+\frac{L_y}{2}} = -\dfrac{j\omega\rho_0}{Z}\left(1 - \dfrac{k_z^{\mathrm{II}}M}{k_0}\right)^2 \psi^{\mathrm{II}}\Big|_{y=+\frac{L_y}{2}}, \end{cases} \tag{4}$$

where ρ_0 is the air density, C_0 the sound speed and $k_0 = \omega/C_0$ the wavenumber. This system (4) referred to a uniform impedance boundary condition over the upper duct wall. k_z^{II} represented the axial wavenumber inside the treated region of the duct (Fig. 5). This unknown did not appear in the boundary equation for the no-flow case and the system was solved by a finite difference discretisation. The axial wavenumbers $k^{i,\pm}_{z,mn}$ in Zone II could then be deduced from the dispersion equation. In the presence of flow, the impedance boundary condition required the knowledge of these axial wavenumbers and different strategies were proposed to overcome this problem, for instance by using an iterative process, or by re-writing a complete system to introduce the axial wavenumbers as additional unknowns. As our main objective was to model the MATISSE test bench which is devoted to plane waves and low Mach numbers (below 0.15), we decided to use the following simplified formulations (5) for the axial wavenumbers in the boundary condition equation of the treated region:

$$k_z^{\mathrm{II}\pm} = \frac{k_0}{1 \pm M}, \tag{5}$$

where M is the Mach number.

This approximation led to the following simplified boundary condition (6), which allowed to solve the same type of system as in the no-flow case and was sufficient to provide the flow influence on the optimal impedance in a first estimation.

$$\frac{d\psi^{\mathrm{II}}}{dy}\Big|_{y=+\frac{L_y}{2}} = -\frac{j\omega\rho_0}{Z}(1-2M)\psi^{\mathrm{II}}\Big|_{y=+\frac{L_y}{2}}. \tag{6}$$

Then, the modal amplitudes A^i_{mn} and B^i_{mn} were resolved with the impedance transport from the anechoic termination to the source plane, according to the generalised matrix model proposed by Roure [23]. Continuity of both potential and its axial derivative were assumed between the different zones. These relations were expressed through transformation matrices whose terms were the projections of eigenfunctions of one zone along the eigenfunctions of the next zone. It can be noticed that amplitudes B^i_{mn} in zone III were zero due to the non-reflective boundary condition on the duct outlet plane. Both pressure and velocity fields can be deduced from relations (7) and (8):

$$p^i(x,y,z) = j\omega\rho_0\Phi^i(x,y,z), \tag{7}$$

$$v^i_z = \frac{\partial\Phi^i(x,y,z)}{\partial z} = \Phi^i_z(x,y,z). \tag{8}$$

The transmission loss is defined as the difference between the incident power level in Zone I and the radiated power level in Zone III. These values were obtained from the resulting values of the modal amplitudes for the (0,0) mode.

3.2. Optimum impedance analysis

The optimum resistance and the optimum reactance of the liner correspond to the real and imaginary parts of Z, respectively, leading to maximum transmission-loss values.

First a 160-mm-long treated region on the upper wall of MATISSE duct was tested. The optimum impedance for various mean-flow velocities is presented in Fig. 6. Results obviously depend on the step in the real and imaginary parts of impedance and successive refinements down to a step of 0.01 led to the present curves. Optimum resistance appeared to increase with frequency, while reactance was negative and decreased over the entire frequency range of interest. Moreover, both values were of the same order, as expected from Cremer's results [15]. The presence of a uniform mean flow inside the duct did not significantly modify either optimum resistance or reactance. Their evolution and values in the frequency range of interest remained similar.

Complementary studies were performed to evaluate the influence of treatment length on optimum impedance. Increasing the liner surface led to curves in agreement with those of Cremer and Tester (Fig. 7). Simulations showed that optimum resistance increased with the length of the treated surface, while optimum reactance was not significantly affected. The longer the liner, however, the higher the optimum attenuation levels. Applying the finite impedance condition to two opposite walls of the MATISSE flow duct, optimum impedance trend was not modified. Both absolute values (resistance and reactance), however, appeared about half those in the reference configuration (same total length but only one treated wall).

3.3. Attenuation sensitivity study

The sensitivity of the transmission loss factor to resistance and reactance variations was analysed in order to characterise the optimum attenuation area, and potentially define a tolerance range for the reproduction stage

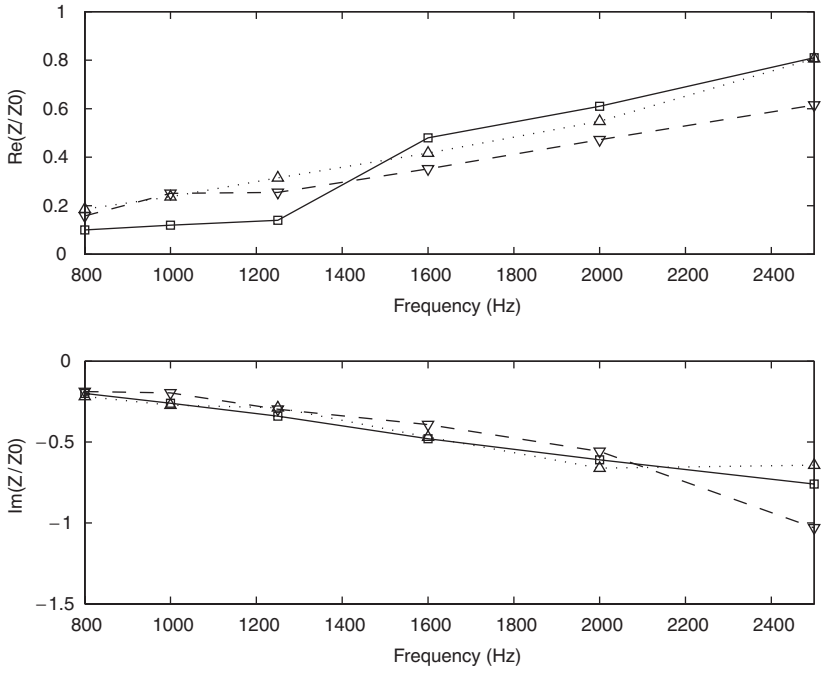

Fig. 6. Influence of the flow velocity on the optimum impedance: no flow (□), mean flow 20 m/s (△), mean flow 50 m/s (▽).

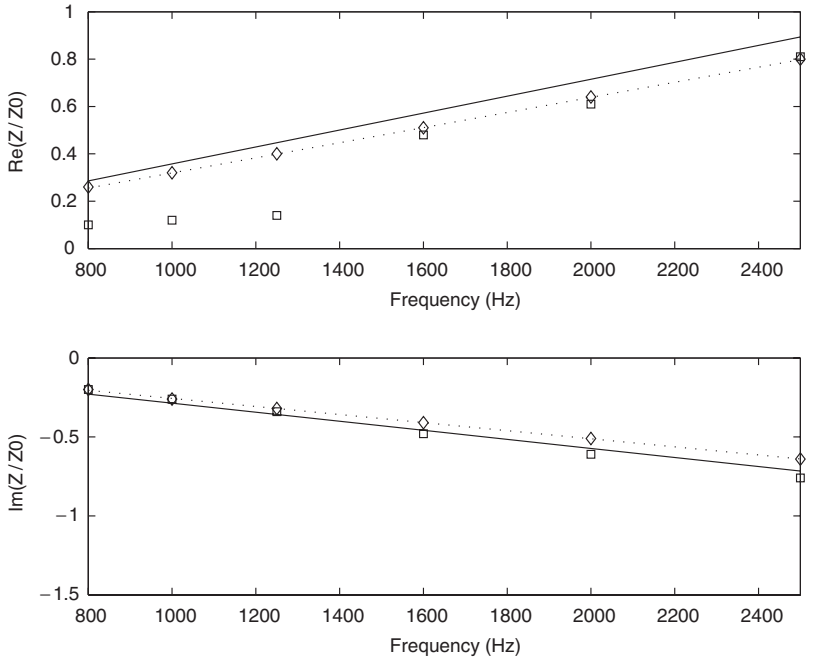

Fig. 7. Comparison between multimodal results (◇) and Cremer's simulation (—) in the no-flow case, comparison between multimodal results (□) and Tester's simulation (- - -) in the case of a mean flow of 20 m/s.

of the target impedance. Fig. 8 represents the transmission loss index plotted in the impedance plane for the no-flow configuration and for various frequencies. The calculation step for the resistance and reactance was set at $0.1Z_0$ in this global analysis and for this reason, small discrepancies could sometimes be found with the optimal values of impedance obtained in the previous section. The optimum attenuation areas, defined as the impedance plane region corresponding to maximum value minus 15 dB, appeared quite small. Their widths reached about $0.2Z_0$ on both axes. Experimental work by Wirt [24] showed attenuation maps leading to similar conclusions: particularly narrow and quasi-circular optimum noise reduction regions. The same maps were plotted for a mean flow velocity of 50 m/s (see Fig. 9). The optimum attenuation areas were smaller in this case. Moreover, more than one optimum area may appear at certain frequencies and flow velocities. This phenomenon is due to the simulation configuration, where a finite (and relatively small) absorbing length is considered. This effect disappears if a finite impedance boundary condition is implemented on the entire upper wall. Therefore, the possible existence of several maximum attenuation areas must be related to the discontinuities introduced at the boundaries between regions due to the finite length of the acoustic treatment.

3.4. Conclusion

Although the optimum impedance values must be calculated for each specific set-up, some general remarks can be derived from the present analysis. It has been demonstrated that both the optimum resistance and reactance depend on several parameters, such as treatment area length and the number of walls covered by the finite impedance condition. Furthermore, higher flow velocities may affect these values. The evolution of the simulated optimum impedance with frequency is in agreement with previous findings by Cremer and Tester. Since both optimum resistance and reactance do not significantly depend on flow for the low velocities considered in the present study, it can be assumed that the optimum impedance obtained in the no-flow case is the target impedance to be achieved at the liner input. However, this value must be precisely reproduced to reach high attenuation levels, especially in the presence of flow.

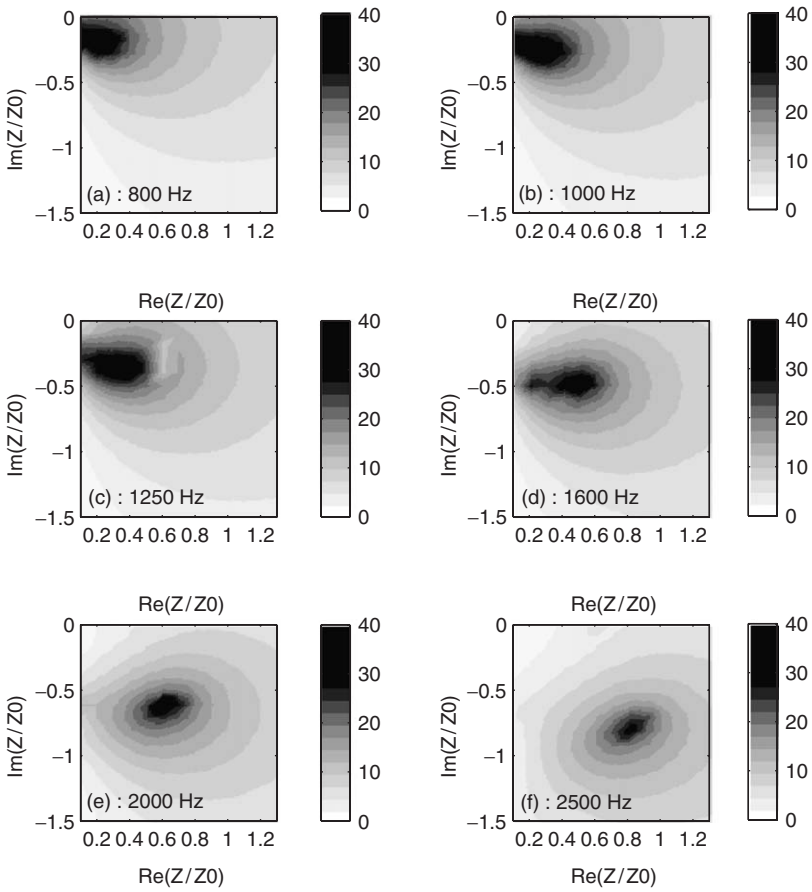

Fig. 8. Sensitivity study: transmission loss predicted in the impedance plane, for different frequencies. No-flow case. (a) 800 Hz, (b) 1000 Hz, (c) 1250 Hz, (d) 1600 Hz, (e) 2000 Hz, (f) 2500 Hz.

4. Selection of the passive layer

The goal of this optimisation stage was to determine the parameters of the porous layer under a rear face boundary condition, leading to the desired surface impedance values. First studies dealing with the selection of a suitable active/passive liner only concerned a precise achievement of the target surface resistance [8]. However, the conclusions of the previous section suggest a non-negligible influence of the optimum reactance, especially in the highest frequency range where quite strongly negative values were reached. Simultaneous achievement of optimum resistance and reactance values is currently being investigated.

The acoustic behaviour of a porous layer has been described by five characteristic parameters as resistivity, porosity, tortuosity and two characteristic lengths (or respective viscous and thermal shape factors, s and s') in the model proposed by Allard [25]. Two additional parameters, the thickness e of the passive layer, and the depth d of the air gap behind the porous sheet, are needed to model the input impedance of the porous sheet, for hybrid liner functioning (see Fig. 2). Considering the large number of parameters involved, the complexity of the function to be minimised and the difficulty of finally finding a material having the target characteristic parameters, we adopted a step-by-step selection process among existing absorbent materials. According to previous analyses, a constant target resistance can be precisely reproduced throughout a large frequency range for thin and highly resistive materials [9] in the active mode. Under these conditions, reactance was very close to zero, and often slightly positive. On the contrary, material thickness should be increased and resistivity reduced to reach a negative decreasing reactance. However, this behaviour afforded higher resistance values than those expected. In order to establish the best compromise to reach the desired impedance values, some

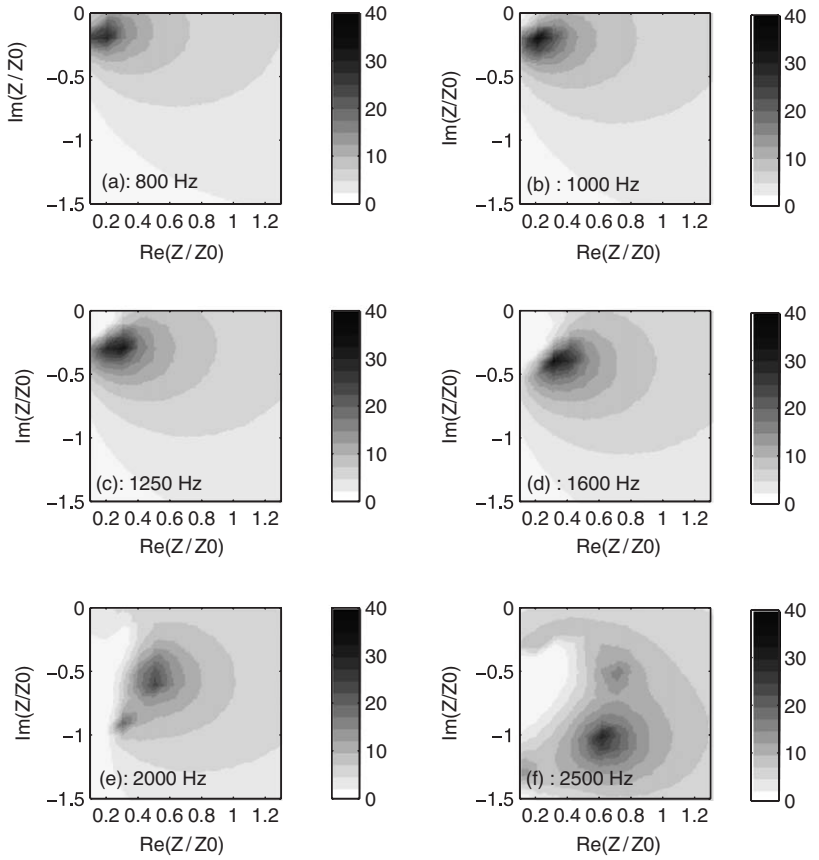

Fig. 9. Sensitivity study: transmission loss predicted in the impedance plane, for different frequencies. Uniform flow 50 m/s. (a) 800 Hz, (b) 1000 Hz, (c) 1250 Hz, (d) 1600 Hz, (e) 2000 Hz, (f) 2500 Hz.

common porous materials in a single or multilayer set-up, with different rear boundary conditions, were successively studied.

The porous media considered in this section had been previously characterised by an inverse acoustic method using standing wave-tube measurements [26]. First, some wire meshes were tested. Such materials are commonly used in turbo-engine nacelle applications. On account of their particular properties (extremely thin and highly resistive layers), these materials show broadband acoustic behaviour. When associated to specific operating conditions, this sort of layer leads to strong noise reduction. When a pressure release condition is achieved on the rear face of a highly resistive material such as a wire mesh, its surface resistance comes to approximately equal its flow resistance $R = \sigma e$. Therefore, an appropriate choice of the product σe enables quite precise reproduction of the target resistance, because the optimum value does not significantly change over the frequency range of interest, as shown in Fig. 6. For the specific MATISSE set-up, a wire mesh manufactured by GANTOIS, with a resistance close to $0.3Z_0$, was selected. However, the related surface reactance appeared slightly positive, whereas the target frequency shape should be negatively decreasing. Wire mesh materials in the active mode were thus not suited to simultaneously achieving both optimum resistance and reactance curves.

Using a single porous layer in active mode was then tested. The modelling of porous media revealed that negative reactance could be achieved but only for materials having a resistance significantly greater than the target value. For instance, Fig. 10 reports the surface impedance of 9-mm-thick rock wool (resistivity $\sigma = 1.3710^5$ rayls/m), backed by a pressure release condition. Such a configuration provided the negative decreasing optimum reactance, but its resistance was rather high ($3Z_0$) compared to the desired mean value (about $0.5Z_0$).

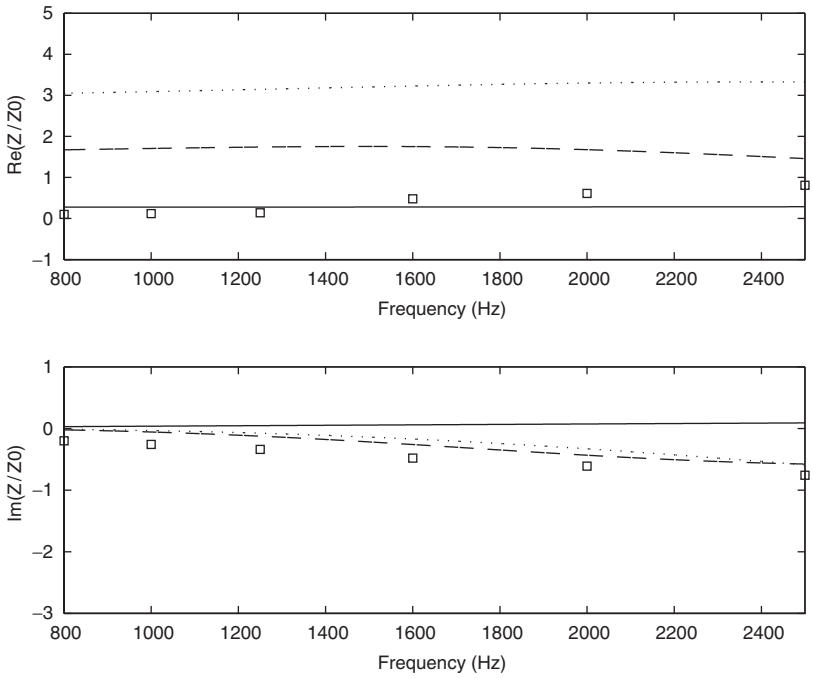

Fig. 10. Surface impedance predictions in active mode: comparison between the optimum impedance for the MATISSE flow duct (□), the wire mesh surface impedance (—), the 9-mm-thick rock wool surface impedance (- - -) and the multilayer wire mesh and 4 mm thick-rock wool surface impedance (— —).

Another study concerned a multilayer configuration. The passive sheet at the input of the hybrid absorber was composed of the wire mesh, a 17-mm-deep air gap and a 4-mm-thick rock wool sample. The wire mesh enabled cell surface resistance to be controlled, while the air gap and rock wool couple provided the desired negative reactance frequency shape. Fig. 10 shows the surface impedance of this multilayer under a pressure release condition. These results represent a fairly accurate reproduction of the imaginary negative decreasing part. However, the real impedance part still remains high ($\approx 1.7Z_0$) as compared to the optimum value, although lower than with the single rock wool layer. Indeed, a low-frequency approximation of the input impedance of such an assemblage is given by

$$\frac{Z}{Z_0} = R_1 + R_2 + \mathrm{j}\,\tan(k_0 d)(1 - R_2^2), \tag{9}$$

where R_1 and R_2 are the specific resistances of the front and back layers, and d the air gap length. Consequently, a negative reactance is obtained for R_2 greater than one, leading to an overly high global resistance.

The passive functioning of the liner was also studied, in order to approximate optimum impedance in the higher frequency range. Surface impedance was predicted for each of the previous porous media backed by a 20-mm-deep air cavity. The results are presented in Fig. 11. The air gap slightly modified the surface resistance of these materials and introduced strongly negative reactance values in the low frequency range. However, at higher frequencies, the imaginary part increased and the surface impedance became similar to the target values.

This theoretical study highlighted the difficulty of simultaneously reproducing both optimum values in the case of the MATISSE flow duct. Thus a compromise between reliable resistance and precise reactance was required so as to be able to select the best-suited passive layer for the hybrid absorber. The new material selection criterion was the sound attenuation achieved.

The simulated transmission loss of the wire mesh and the multilayer configuration, both backed by an active boundary condition (pressure release), are reported in Fig. 12. In the low frequency range, below 1.6 kHz, the

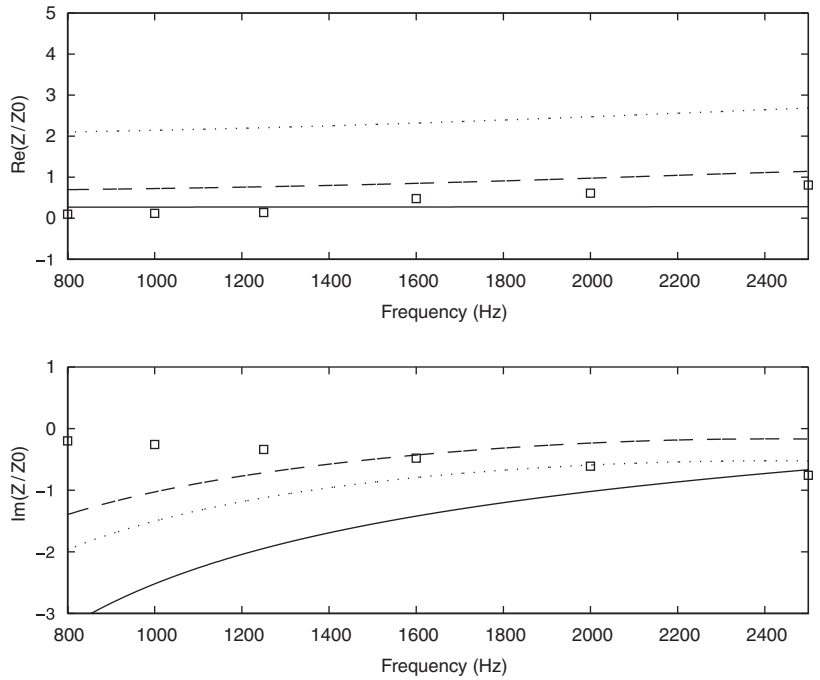

Fig. 11. Surface impedance predictions in passive mode (0.02 m deep back cavity): comparison between the optimum impedance for the MATISSE flow duct (□), the wire mesh surface impedance (—), the 9-mm-thick rock wool surface impedance (- - -) and the multilayer wire mesh and 4-mm-thick rock wool surface impedance (— —).

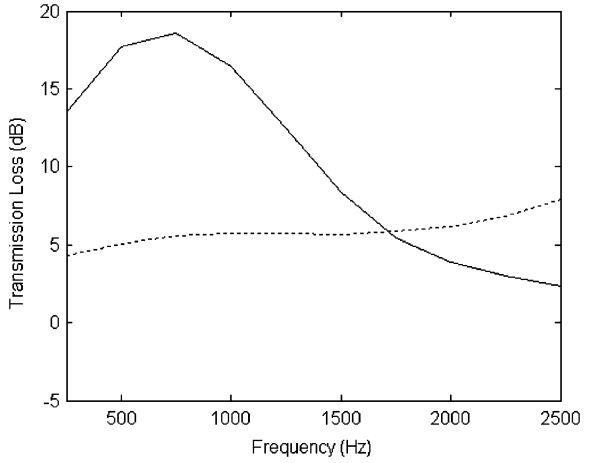

Fig. 12. Transmission loss simulations for acoustic treatments placed on MATISSE upper wall over 160 mm: calculations using surface impedance predictions with a pressure cancellation rear face boundary condition. Wire mesh (—), multilayer composed of the wire mesh and the 4-mm-thick rock wool (- - -).

selected wire mesh seemed to be the most effective solution, giving greater attenuation. Achieving target resistance was a critical factor for low frequencies, provided that reactance remained weak. Nevertheless, as frequency increased, the performance of the wire mesh sheet decreased sharply and the noise reduction with the multilayer configuration became more significant. Fig. 13 compares the transmission loss obtained with the same wire mesh for the active mode and for three passive boundary conditions (10–15 and 20-mm-deep air cavities). These curves reveal the benefit of combining passive and active techniques to improve noise

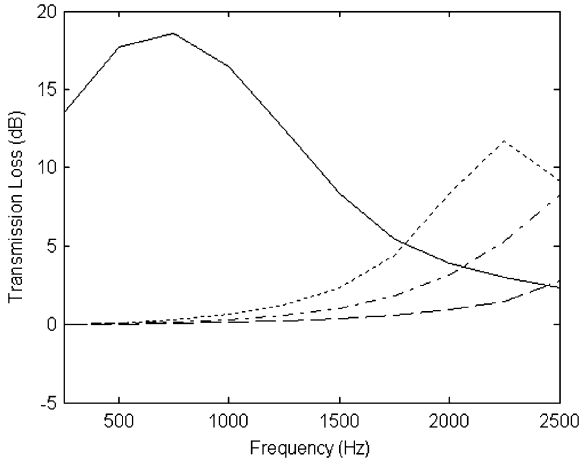

Fig. 13. Transmission loss simulations for the wire mesh placed on MATISSE upper wall over 160 mm: comparison between the active mode (—) and three passive rear face boundary conditions: a 10 mm deep air cavity (— —), a 15-mm-deep air cavity (– - –) and a 20-mm-deep air cavity (- - -).

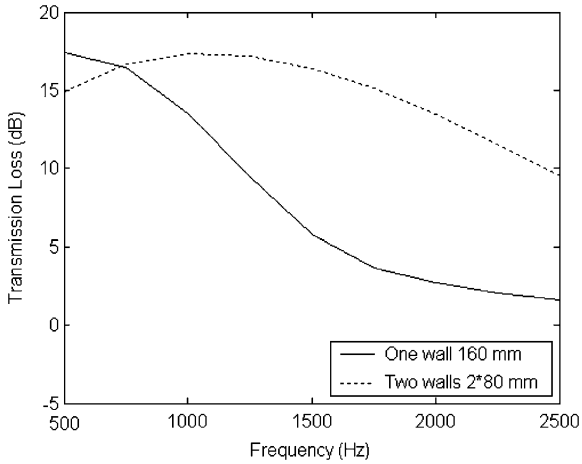

Fig. 14. Transmission loss simulations for the wire mesh placed on MATISSE upper wall (—) and split on both opposite walls (- - -). Active mode.

reduction over a wider frequency range. In this high frequency range, achieving optimum reactance appears to be the critical factor. A cut-off frequency between active and passive functioning modes can be determined for each particular set-up (material properties and air cavity depth). With the 20-mm-thick air gap, for instance, the shift from active to passive mode is at 1.8 kHz. Greater attenuation levels can be obtained covering longer surfaces on the upper wall or, as shown in Fig. 14, with the same total area on both opposite walls, although the complete optimisation procedure was not replicated for these configurations.

5. Experimental validation

The theoretical results from previous sections were experimentally verified. Four prototype hybrid cells (Fig. 15) were manufactured by METRAVIB to be tested on the MATISSE flow duct under grazing acoustic incidence. Each hybrid absorbent cell was composed of a passive layer and an active control system. The passive layer on the front face of the cell was the selected wire mesh backed by a metallic grid to avoid any

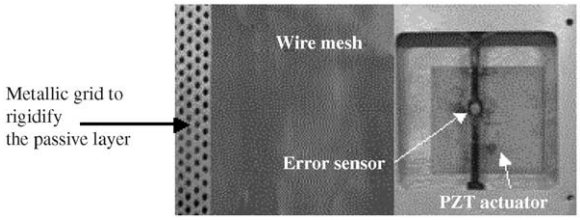

Fig. 15. One hybrid cell prototype.

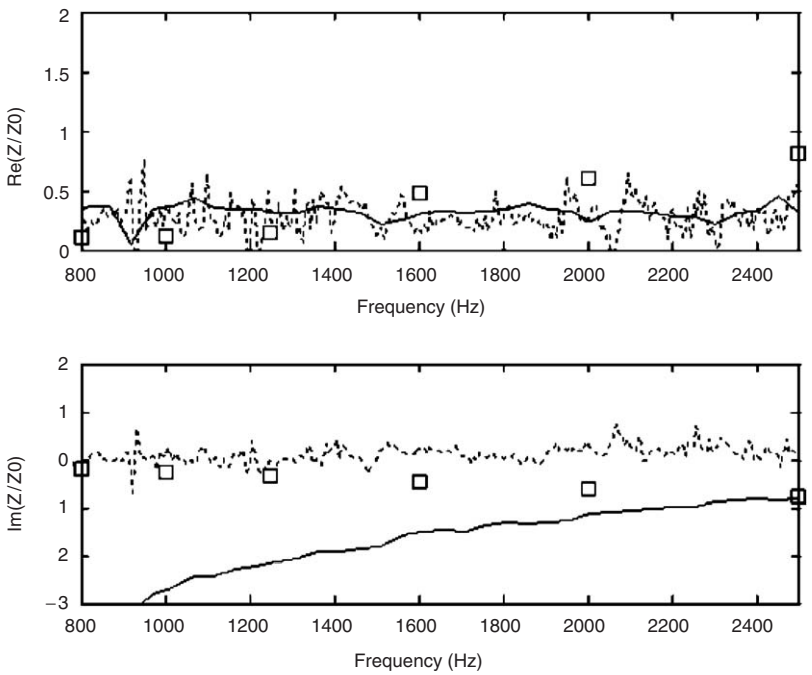

Fig. 16. Surface impedance measurements in the standing wave tube: comparison between the optimum impedance for the MATISSE flow duct (□), and measured surface impedance of the wire mesh layer backed by a 20-mm-deep air cavity (—) or backed by a pressure cancellation boundary condition (- - -).

undesirable bending of the material. The active control system of each cell consisted of an error microphone, a secondary source and a digital filtering algorithm downloaded on a dSPACE-DS1103 controller board. The error microphone (Knowles FG-3329) was centred in the cavity behind the passive multilayer (wire mesh + grid) to ensure the pressure release condition over the largest possible area [10]. The secondary source was composed of an aluminium plate excited by a piezoceramic patch. A feedback control algorithm was specially developed to operate independently cell by cell so as to minimise all error signals. More details about the active system are available in Refs. [10,11]. Each hybrid cell prototype covers an effective area of nearly $55 \times 55\,\mathrm{mm}^2$.

Initially, a hybrid cell prototype was subjected to normal acoustic incidence in a standing wave tube to check surface impedance against the predicted value. Experimental results for cell surface impedance in the active and in the passive 20-mm-deep air cavity mode are plotted in Fig. 16. Both curves are compared to the target optimum impedance. As discussed above, when the active boundary condition was achieved, the hybrid absorber surface resistance was close to the optimum value mainly in the low-frequency domain. The reactance was almost zero and the discrepancy with respect to the optimum imaginary part increased with frequency. In the passive boundary condition, surface reactance, although strongly negative at low

frequencies, became almost optimal at higher frequencies. The theoretical predictions for optimum impedance were experimentally validated.

5.1. Experimental setup

Experiments on such hybrid cells under grazing acoustic incidence were conducted in the MATISSE flow duct (Fig. 17), already described in Section 2. Two couples of B&K $1/4''$ microphones were flush-mounted upstream (M1,M2) and downstream (M3,M4) of the test section, to further estimate the performance indices (Fig. 3). The primary acoustic source—a loudspeaker enclosed in a wooden box filled with rock wool—was located in a side-branch configuration over the upper wall of the main duct. This source was driven by either pure tones or swept sine signals, ensuring a sufficient signal-to-noise ratio at high flow velocities. Noise levels inside the MATISSE flow duct ranged from 110 to 120 dB. The tested flow velocities were quite low: up to 50 m/s ($M = 0.15$). The frequency bandwidth of interest was reduced to the plane wave range, set from 0.7 to 2.5 kHz.

The transmission loss index was estimated with a set of three flush-mounted microphones. The pressure signals at microphones M1 and M2 were recorded to extract the incident wave component I, inside zone I of the duct. Due to the anechoic termination, only one signal (from M3 for example) was necessary to obtain the transmitted wave component T. Coherence between signals was checked in all tests. Accordingly, the experimental transmission loss value was deduced from

$$\mathrm{TL} = 20\,\log\left|\frac{I}{T}\right|. \tag{10}$$

Before starting the experiments, the anechoic termination of the MATISSE set-up was experimentally confirmed. The reflection coefficient inside the flow duct was estimated from signals picked either up at microphones M1/M2 or M3/M4, without any acoustic treatment. It was lower than 0.1 over the entire frequency range, even in the most critical case (for flow velocity 50 m/s).

Several configurations were tested on the upper wall of the duct in order to validate the general concept of hybrid absorption. Note that only results concerning the selected wire mesh sheet are presented here. Both the passive and active functioning modes of the four hybrid cell prototypes were checked for an acoustic treatment of the same size (effective length = 220 mm).

5.2. Measurements in the passive mode

The first result involved the passive behaviour of a conventional treatment (sdof liner). In this case the wire mesh was backed by a 17 mm deep honeycomb having 9 mm wide cells. A swept sine signal

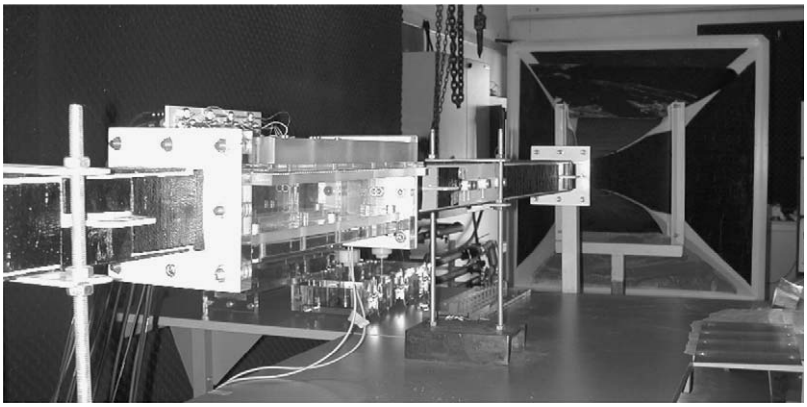

Fig. 17. MATISSE experimental facility.

from 0.7 to 2.5 kHz with a step of 0.2 kHz was used. Fig. 18 shows the transmission loss obtained for different flow velocities. As expected, the attenuation is very poor at low frequencies but strongly increasing with the frequency. The liner performance at higher frequencies seems to be slightly superior in the presence of flow.

The next experiment was devoted to testing the performance of the hybrid cells in the passive mode, with a 20-mm-deep air gap. Transmission losses for the various flow velocities are plotted in Fig. 19. Once more, the passive behaviour was confirmed. As expected, higher attenuation levels were reached, since the air cavity was greater. The flow effect remained negligible. The greatest sound reduction was obtained at 2.3 kHz, where the impedance achieved by the treatment is very close to target for both the real and imaginary parts, as can be seen on Fig. 16.

In conclusion, the passive behaviour of the prototype was in agreement with predictions. Moreover, the hypothesis underlying the calculations, i.e., that the absorber behaves as a locally reacting material, was confirmed.

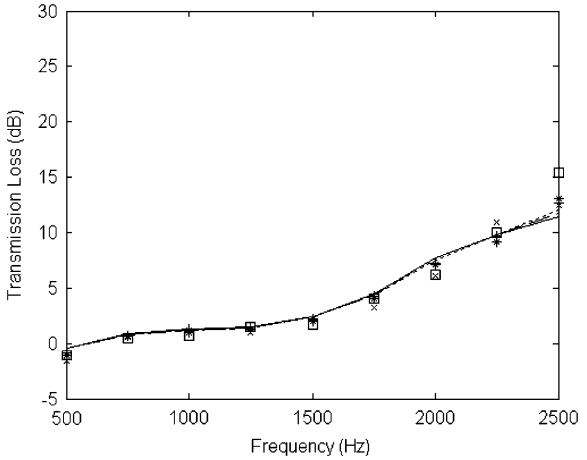

Fig. 18. Transmission loss for the passive sdof treatment at different flow velocities. No flow (—), flow 5 m/s (— —), flow 10 m/s (- - -), flow 20 m/s (+), flow 30 m/s (∗), flow 40 m/s (×), flow 50 m/s (□).

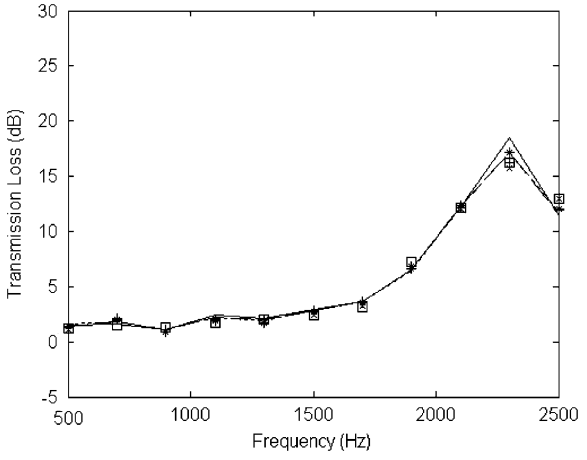

Fig. 19. Transmission loss measurements for the passive functioning mode of the hybrid cells, for different flow velocities until up to 50 m/s. No flow (—), flow 5 m/s (— —), flow 10 m/s (- - -), flow 20 m/s (+), flow 30 m/s (∗), flow 40 m/s (×), flow 50 m/s (□).

5.3. Measurements in the active mode

The frequency range to test the active functioning mode of the hybrid absorber was set from 0.7 to 1.9 kHz. As discussed in the theoretical study, above this upper frequency the passive solutions become more effective. Fig. 20 represents the measured transmission losses obtained for flow velocities between 0 and 50 m/s, when the active control system on the rear porous layer face is turned on. As expected, considerable noise reduction was obtained at low frequencies (from 20 to 25 dB at 0.7 kHz), whereas the attenuation sharply decreased as frequency increased. The presence of flow did not significantly modify the experimental transmission loss, except from the lower frequency range where it was reduced as flow velocity increased. The experimental results were in agreement with the predicted curves. The outcome of reducing the treated area (using only two active cells) is shown in Fig. 21: the longer the treated surface, the greater the attenuation, as predicted theoretically.

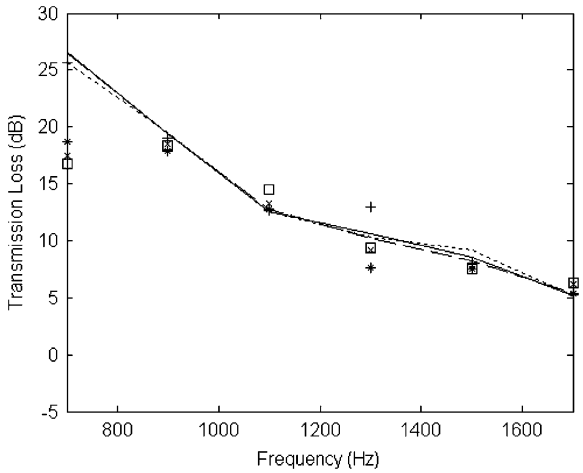

Fig. 20. Transmission loss measurements for the active functioning mode for different flow velocities: No flow (—), flow 5 m/s (— —), flow 10 m/s (- - -), flow 20 m/s (+), flow 30 m/s (∗), flow 40 m/s (×), flow 50 m/s (□).

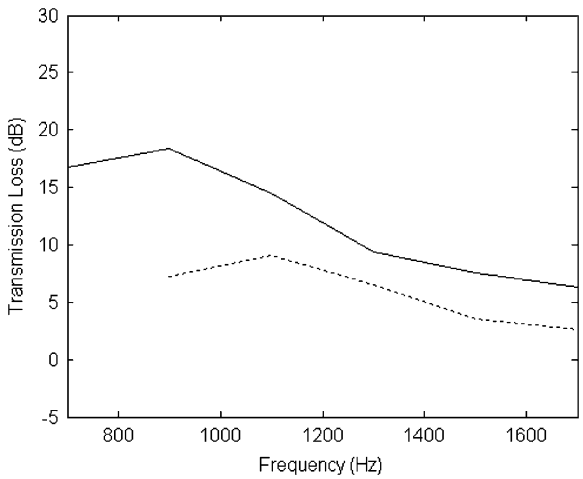

Fig. 21. Transmission loss measurements for the active functioning mode for different treated surfaces: 4 active cells (—) and 2 active cells (- - -), flow velocity 50 m/s.

5.4. Hybrid absorption

Finally, the hybrid functioning of the absorbent prototype was considered. Figs. 22 and 23 superimpose the measured and predicted transmission-loss parameters in both active and passive functioning modes in the no-flow configuration and for a mean flow velocity of 50 m/s, respectively. The experimental results agreed with the predictions, with an effective length of 190 mm for the treatment, instead of the real value of 220 mm. A possible reason is that the pressure reduction was not uniform at the rear face of the wire mesh. Indeed, pressure was minimised at the site of the error microphone, in the centre of each cell. However, measurement showed that, under grazing incidence, the effectiveness of control was significantly reduced at the cell edges. Another possible reason is that reflections encountered with a liner having splices like the hybrid treatment lead to reduced effectiveness. In fact, all the differences from an ideal uniform impedance boundary condition were taken into account by reducing the treated area by a ratio of 0.86. According to the theoretical study, the experimental cut-off frequency could be set at 1.8 kHz in the no-flow condition, and was not greatly modified for higher flow velocities. Both graphs validate the hybrid absorption concept, since significant attenuation

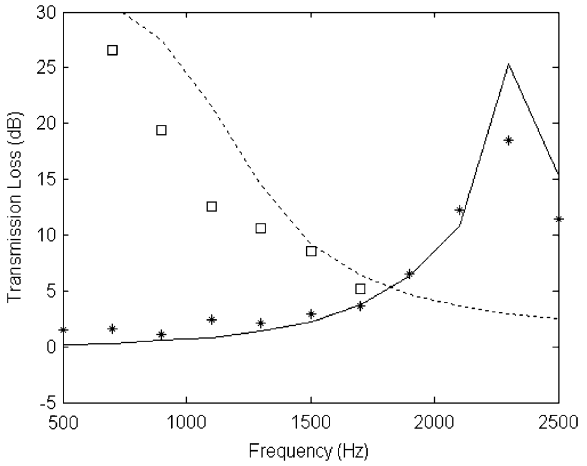

Fig. 22. Comparison between transmission loss predictions and measurements for the hybrid functioning of the cells (no-flow condition): active mode simulation (- - -), active mode measurement (□), passive mode simulation (—), passive mode measurement (∗).

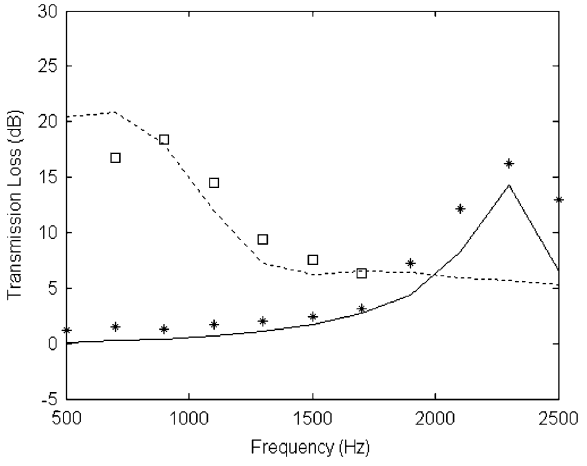

Fig. 23. Comparison between transmission loss predictions and measurements for the hybrid functioning of the cells (flow 50 m/s): active mode simulation (- - -), active mode measurement (□), passive mode simulation (—), passive mode measurement (∗).

levels were achieved throughout the frequency bandwidth: up 25 dB at 0.7 kHz for the active boundary condition and up to 18 dB at 2.4 kHz for the passive boundary condition.

6. Conclusions

A hybrid active/passive treatment was designed to provide broadband noise reduction in flow duct applications. A general procedure to optimise the absorbent cell in a specific laboratory facility was developed. A highly resistive sheet composed of a wire mesh with a resistance close to a third of characteristic air impedance was found to be the most suitable passive layer configuration for any flow velocity up to 50 m/s. The optimum cut-off frequency between the active and the passive functioning mode was determined as 1.8 kHz. The hybrid absorption concept was completely validated, both theoretically and experimentally, since significant sound attenuation was obtained in both the low (up to 25 dB at 0.7 kHz) and high frequency range (up to 20 dB at 2.4 kHz). Attenuation fell to 6 dB in the middle frequency range because the selected configuration resulted from a compromise over the whole frequency range. A sensitivity study showed that the optimum impedance must precisely be reproduced to reach high attenuation levels. Consequently, future work will focus on implementing liners of variable and frequency-dependent impedance, combining active and passive means. A multilayer prototype with an error sensor in the air space between the two porous layers appears suitable for approaching both optimum resistance and reactance curves. The liner optimisation procedure proposed and carried out in this paper could be applied to any more complex test-bench or industrial application. However, the characteristics of each new set-up should be taken account of in calculating the optimum impedance. Moreover, more robust and realistic models should be implemented for complex flow profiles and higher propagation modes. The hybrid liner concept could also be applied in other hostile environments, such as hot streams, by selecting a resistive acoustic layer also integrating thermal isolation properties. Likewise, the porous layer could, in addition to the passive absorption, provide a means of protection against shock and air or liquid flow for the active system.

Acknowledgements

This research was supported by the European Community, under the Silence(r) project (GRD1-2000-25297). The authors acknowledge Fundación la Caixa and the French Government for funding the post-doctoral fellowship of Maria Cuesta at the Centre Acoustique du LMFA (Ecole Centrale de Lyon).

References

[1] H.F. Olson, E.G. May, Electronic sound absorber, *Journal of the Acoustical Society of America* 25 (1953) 1130–1136.
[2] D. Guicking, E. Lorenz, An active sound absorber with porous plate, *Journal of Vibration and Acoustics* 106 (1984) 389–392.
[3] F.P. Mechel, Hybrider Schalldämplfer, Patent No DE4027511.
[4] D. Thenail, Contrôle actif d'impédance et optimisation des performances d'un matériau poreux, PhD Thesis, Ecole Centrale de Lyon, Ecully, France, 1995.
[5] M. Furstoss, D. Thenail, M.A. Galland, Surface impedance control for sound absorption: direct and hybrid passive/active strategies, *Journal of Sound and Vibration* 203 (2) (1997) 219–236.
[6] S. Beyene, A. Burdisso, A new passive/active noise absorption system, *Journal of the Acoustical Society of America* 101 (3) (1997) 1512–1515.
[7] P. Cobo, J. Pfretzschner, M. Cuesta, D.K. Anthony, Hybrid passive–active absorption using microperforated panels, *Journal of the Acoustical Society of America* 116 (4) (2004) 2118–2125.
[8] M.-A. Galland, P. Souchotte, P. Ladner, T. Mazoyer, Experimental investigation of noise reduction in a flow duct through hybrid passive/active liner, *Proceedings of the 7th AIAA/CEAS Aeroacoustics Conference*, Maastricht, The Netherlands, 28–30 May 2001, AIAA Paper 2001-2221.
[9] M.-A. Galland, N. Sellen, O. Hilbrunner, Noise reduction in a flow duct by active control of wall impedance, *Proceedings of the 8th AIAA/CEAS Aeroacoustics Conference*, Breckenridge, Colorado, 17–19 June 2002, AIAA Paper 2002-2213.
[10] O. Hilbrunner, M.A. Galland, N. Sellen, J. Perisse, Optimisation of a hybrid acoustic liner for noise reduction of engine aircraft nacelles, *Proceedings of ACTIVE 2002—The 2002 International Symposium on Active Control of Sound and Vibration*, Vol. 1, Southampton, UK, 2002, pp. 657–668.
[11] B. Mazeaud, N. Sellen, M.A. Galland, Design of an adaptive hybrid liner for flow duct applications, *Proceedings of the 10th AIAA/CEAS Aeroacoustics Conference*, Manchester, UK, 10–12 May 2004, AIAA Paper 2004-2852.

[12] N. Sellen, M. Cuesta, M.-A. Galland, Passive layer optimization for active absorbers in flow duct applications, *Proceedings of the 9th AIAA/CEAS Aeroacoustics Conference*, Hilton Head, South Carolina, 12–14 May 2003, AIAA Paper 2003-3186.
[13] P.M. Morse, K.U. Ingard, *Theoretical Acoustics*, Princeton University Press, Princeton, NJ, 1968.
[14] M.L. Munjal, *Acoustics of Ducts and Mufflers. With Application to Exhaust and Ventilation System Design*, Wiley, New York, 1987.
[15] L. Cremer, Theorie des Luftschall-Dampfung im Rechteckkanal mit schluckender Wand und das sich dabei ergebende hochste Dampfungsmass (in German), Theory regarding the attenuation of sound transmission by air in a rectangular duct with an absorbing wall, and the maximum attenuation produced during this process, *Acustica* 2 (1953) 249–263.
[16] B.J. Tester, The propagation and attenuation of sound in lined ducts containing uniform or plug flow, *Journal of Sound and Vibration* 28 (2) (1973) 151–203.
[17] Y. Aurégan, R. Starobinski, V. Pagneux, Influence of grazing flow and dissipation effects on the acoustic boundary conditions at lined wall, *Journal of the Acoustical Society of America* 109 (1) (2001) 59–64.
[18] M.K. Myers, On the acoustic boundary condition in the presence of flow, *Journal of Sound and Vibration* 71 (3) (1980) 429–434.
[19] G. Zlavog, W. Eversmann, Source effects on realized attenuation in lined ducts, *Proceedings of the 9th AIAA/CEAS Aeroacoustics Conference*, Hilton Head, South Carolina, 12–14 May 2003, AIAA Paper 2003-3247.
[20] R.E. Motsinger, R.E. Kraft, Design and performance of duct acoustic treatment, Vol. 2: noise control, in: H.H. Hubbard (Ed.), *Aeroacoustics of Flight Vehicles. Theory and Practice*, 1995, pp. 165–206 (Chapter 14).
[21] Y. Ozyoruk, L.N. Long, Time-domain calculation of sound propagation in lined ducts with sheared flows, *AIAA Journal* 38 (5) (2000) 768–773.
[22] W. Eversman, Effect of boundary layer on the transmission and attenuation of sound in an acoustically treated circular duct, *Journal of the Acoustical Society of America* 49 (5) (1971) 1372–1380.
[23] A. Roure, Propagation du son dans des conduits à section variable. Application à la détermination des fréquences propres de certains volumes complexes, *Euromech 94, L.M.A. Marseille*, 12–15 September 1977.
[24] L.S. Wirt, Analysis, testing, and design of lined ducts, *Journal of the Acoustical Society of America* 51 (5) (1972) 1448–1463.
[25] J.-F. Allard, *Propagation of Sound in Porous Media: Modelling Sound Absorbing Materials*, Elsevier, Amsterdam, 1993.
[26] N. Sellen, M.-A. Galland, O. Hilbrunner, Identification of the characteristic parameters of porous media using active control, *8th AIAA/CEAS Aeroacoustics Conference*, Breckenridge, CO, 17–19 June 2002, AIAA Paper 2002-2504.